HHS Public Access

Author manuscript

Cell Signal. Author manuscript; available in PMC 2022 February 24.

Published in final edited form as:

Cell Signal. 2021 October ; 86: 110078. doi:10.1016/j.cellsig.2021.110078.

TMEM97 ablation aggravates oxidant-induced retinal degeneration

Hongtao Shen[a,1], **Jing Li**[a,1], **Tyler Heisler-Taylor**[b], **Ryan Makin**[c,d], **Huan Yang**[e], **Timur A. Mavlyutov**[e], **Bradley Gelfand**[c,d,f], **Colleen M. Cebulla**[b,*], **Lian-Wang Guo**[a,d,**]

[a]Department of Surgery, School of Medicine, University of Virginia, Charlottesville, VA 22908, USA

[b]Department of Ophthalmology and Visual Sciences, The Ohio State University, Columbus, OH 43212, USA

[c]Center for Advanced Vision Science, School of Medicine, University of Virginia, Charlottesville, VA 22908, USA

[d]Department of Ophthalmology, School of Medicine, University of Virginia, Charlottesville, VA 22908, USA

[e]Department of Surgery, University of Wisconsin, Madison, WI 53705, USA

[f]Department of Biomedical Engineering, School of Medicine, University of Virginia, Charlottesville, VA 22908, USA

Abstract

The retinal pigment epithelium (RPE) is critical to the survival of the overlying photoreceptors. Subject to light exposure and active metabolism, the RPE and photoreceptors are particularly susceptible to oxidative damage that plays an important part in age-related macular degeneration (AMD). Recent meta-analyses identified TMEM97 as a new putative AMD risk locus, though it is yet to be functionally verified. The role of TMEM97 in the retina and RPE is not known. Here we investigated TMEM97 function using the sodium iodate model of oxidant-induced retinal degeneration in TMEM97 knockout (KO) mice. We found markedly increased reactive oxygen species (ROS) and loss of photoreceptos in TMEM97 KO mouse retinas relative to wild type (WT) controls. *In vitro*, sodium iodate treatment of CRISPR-mediated TMEM97 KO RPE cells resulted in diminished abundance of the master antioxidant transcription factor NRF2 and its target gene product SOD2, the mitochondrial superoxide dismutase, as well as elevated ROS and

*Corresponding author. colleen.cebulla@osumc.edu (C.M. Cebulla). **Corresponding author at: L W Guo, Department of Surgery, School of Medicine, University of Virginia, 409 Lane Rd, Charlottesville, VA 22908, USA. lg8zr@virginia.edu (L.-W. Guo).

[1] These authors contributed equally to this work.

Author Contributors

HS: Investigation, formal analysis, methodology. JL: Investigation, formal analysis. THT: Investigation, formal analysis. RM: Investigation. HY: Resources, methodology. TAM: Investigation. BG: Resources, writing - review & editing. CMC: Conceptualization, writing- reviewing and editing. LWG: Conceptualization, writing- original draft, reviewing, and editing.

Competing Interests

Dr. Gelfand is named as an inventor on patent applications on macular degeneration filed by the University of Virginia, and is cofounder of DiceRx.

Appendix A. Supplementary data

Supplementary data to this article can be found online at https://doi.org/10.1016/j.cellsig.2021.110078.

apoptosis markers. Moreover, TMEM97 KO affected proteins key to mitochondrial and lysosomal stability and impeded autophagy flux. These findings suggest that the absence of TMEM97 in RPE cells disturbs redox-balancing systems, thereby heightening oxidative stress. As TMEM97 is a druggable target, this study may inspire interest in basic and translational research in the context of retinal degeneration.

Keywords

TMEM97; Retina; RPE; Photoreceptor; Oxidative stress; Mitochondria; Lysosome

1. Introduction

Reactive oxygen species (ROS) are integral to normal cellular signaling. However, imbalance in ROS production and removal begets excessive oxidative stress leading to a broad-spectrum of disorders, especially age-related diseases. A prominent example is age-related macular degeneration (AMD), a major cause of blindness in developed countries. A key hallmark of AMD is degeneration of the retinal pigment epithelium (RPE) in association with oxidative damage and the ensuing loss of the overlying photoreceptors [1]. Unfortunately, clinical trials with antioxidant supplements have shown limited benefits [1]. In fact, it is increasingly recognized that the use of antioxidants that nonspecifically cleanse both physiologic and pathologic ROS can be detrimental [1,2]. Endogenous self-protective regulators within the RPE, which neutralize oxidative stress within the cell, hold promise as specific targets for effective therapeutic options for conditions linked to oxidative damage [3,4].

Recent meta-analyses of genome–/transcriptome-wide association studies (GWAS/TWAS) identified *TMEM97* (transmembrane protein 97) as a putative new AMD risk locus, although functional verification is still lacking [5,6]. Of the few functional studies of TMEM97, most have focused on its expression and role in cancer cells; its molecular function is not well characterized. Recent literature implicates its involvement in cholesterol homeostasis and Niemann-Pick disease [7–9].

Separately, with its coding gene unknown, the sigma-2 receptor (S2R) [10] had been pharmaceutically targeted for decades in treating psychotic disorders [11]. Very recently, this coding gene was identified to be *TMEM97* [12]. Serendipitously, TMEM97 thus became targetable, with experimental compounds in clinical trials or drugs used in practice that act on S2R [13–15], unlocking the potential for clinical intervention. Indeed, S2R ligands showed neuroprotective benefits in preclinical tests (*e.g.* Alzheimer's disease) and clinical trials [13,15], and even a potential for treating COVID-19 [16]. On the other hand, reports revealed off-targets of some S2R ligands [17] or TMEM97-independent ligand activity [18], underscoring the importance of determining TMEM97(S2R) functions using genetic approaches. Moreover, the role of TMEM97 in the retina remains unclear.

We observed prominent TMEM97 expression in human and mouse RPE. To investigate its potential role in the retina and RPE, here we used a TMEM97 knockout (KO) mouse line. To induce oxidative retinal degeneration, we performed tail-vein injection of sodium iodate

($NaIO_3$). This is a well-characterized model whereby $NaIO_3$ selectively damages the RPE resulting in photoreceptor loss, hence recapitulating some basic features of AMD [19–21]. Evidence indicates that $NaIO_3$ induces RPE cell apoptosis involving endoplasmic reticulum stress response pathways such as X-box-binding protein 1 [22]. Interestingly, we observed increased RPE damage and photoreceptor loss in TMEM97 KO (*vs* WT) mice treated with $NaIO_3$. Similarly, knockout of TMEM97 in RPE cells *in vitro* exacerbated oxidative stress and destabilization of nuclear factor erythroid 2-related factor 2 (NRF2) as well as organelles (mitochondria and lysosomes) whose dysfunction elevates ROS [23]. To the best of our knowledge, this is the first report of genetic evidence suggesting that TMEM97 is a novel regulator of endogenous antioxidant processes.

2. Materials and methods

2.1. Materials

The sources of major reagents are listed in Table S1, or otherwise specifically stated below.

2.2. Ethics statement

All studies on human tissues followed the guidelines of the Declaration of Helsinki. The study of deidentified tissues from deceased individuals obtained from various eye banks in the United States was exempted from IRB review by the University of Virginia Institutional Review Board for Health Sciences Research in accordance with U.S. Health & Human Services human subject regulations. All animal procedures were approved by the Institutional Animal Care and Use Committee, and were performed in accordance with the association for research in vision and ophthalmology (ARVO) statement for the Use of Animals in Ophthalmic and Vision Research. Mice were maintained on a 4% fat diet (Harland Teklad, 8604 M/R) with standard light/dark cycles (12h/12h). Age-matched male mice (40–50 days old) were used. To induce RPE degeneration and associated photoreceptor loss, we used the established model of systemic delivery of $NaIO_3$, which is a potent oxidant [19–21]. Mice received single tail-vein injection of $NaIO_3$ (30 mg/kg of body weight, from Sigma-Aldrich) or PBS control [22]. Injection was performed under isoflurane anesthesia (through inhalation, flow rate 2ml/min). Animals were euthanized at post-injection day 3 in a chamber gradually filled with CO_2.

2.3. Immunohistochemistry using human retinal tissues

Eyes from individuals without a history or evidence of retinal disease upon gross examination were obtained within 12 h of death and preserved in formalin and embedded in paraffin. Five-micron thick sections were prepared for immunohistochemistry by bleaching pigment using oxalic acid/potassium permanganate solution followed by heat-induced epitope retrieval with Tris-EDTA buffer (pH 9) at 60 °C for 1 h. Immunohistochemical staining of bleached eye sections was performed with rabbit anti-human TMEM97 antibody (Proteintech Cat. No. 26444–1-AP, diluted 1:100 in DAKO antibody diluent) overnight at 4 °C. Rabbit IgG isotype control was applied to adjacent sections in place of the primary antibody to ascertain the specificity of staining. Slides were incubated with a biotin-conjugated secondary antibody, followed by incubation with VECTASTAIN® ABC-AP reagent and development using Vector Blue (Vector Laboratories, Cat No. AK-5000

and SK-5300, respectively). Images were obtained using an Olympus VS120-S6-W slide-scanning microscope.

2.4. TMEM97 knockout mice

To establish a TMEM97 KO mouse colony, cryoprotected sperms of the *C57BL/6N-Tmem97*$^{tm1.1(KOMP)Vlcg}$ strain were purchased from the KOMP Repository at UC Davis (stock#10753A-D5). The strain was revived at the Ohio State University Genetically Engineered Mouse Modeling Core, on the background of C57BL/6 J (JAX#000664) and backcrossed for at least 9 times. Homozygous KO and WT littermates from heterozygous breeders were used in experiments. In normal conditions, these littermates showed no overt phenotype in appearance and body size. Their genotypes were confirmed by PCR using primers as the following: WT(f) (GGGTAACATTTGAATTATGGCTAG) and WT(r) (CACACTGGGGGCTCCTGCATC), to detect a 464-bp WT *Tmem97* sequence; KO(f) (ACTTGCTTTAAAAAACCTCCCACA) and KO(r) (GGTGTCACACACCTTTAATCCCAGC), responsible for a 722-bp deleted sequence.

2.5. Spectral domain optical coherence tomography (SD-OCT)

The mice treated with PBS or $NaIO_3$ (30 mg/kg, tail-vein injected) were anesthetized *via* i.p. injection of ketamine-xylazine (90 mg/kg ketamine mixed with 10 mg/kg xylazine) with topical tetracaine eye drops (0.5%) for additional topical numbing. For live animal imaging, the mouse was restrained in place on a platform, and its eyes were dilated with topical tropicamide drops (1%). Animals were kept on a heated pad until observed to wake. SD-OCT was performed on mice on both eyes using a Leica/Bioptigen Envisu R2200 SDOIS, a mouse bore lens, the InVivoVue 2.4.34 software, and the InVivoVue Diver 3.3.7 software. On each eye, three scans were acquired centered on the optic nerve: a 1.4 mm 1000x1x60 frames (1000 A-scans per B-scan, 1 B-scan, 60 B-scans per frame) linear B-scan for high quality images, a 1.4 × 1.4 mm 1000x6x25 frames radial scan for data collection, and a 1.4 × 1.4 mm 400x400x4 frames volumetric scan for volume intensity projection (VIP) views. Retinal layers were measured using auto-segmentation and manual marker segmentation in the Diver software.

2.6. Cryosection preparation, histology, and bright-field microscopy

Enucleated mouse eyes were fixed at 4 °C overnight in 4% paraformaldehyde and cryoprotected with sucrose (30% in PBS). Cryosections of 12 μm each were cut from the eyeballs frozen in optimum cutting temperature embedding medium (Sakura Finetek USA, Inc., Torrance, CA). The sections were stained with haematoxylin and eosin (H&E). High and low magnification images were acquired within 200 μm of the optic nerve head (on both sides) with a Nikon microscope. The ONL thickness was manually measured.

2.7. Confocal fluorescence microscopy

We followed the method in our previous report [24]. Briefly, enucleated eyes were fixed overnight in 4% paraformaldehyde and cryoprotected with 30% sucrose. Cryosections of 12 μm each were cut. The sections were permeabilized with 0.1% Triton X-100 in PBS

for 20min, blocked with 5% normal donkey serum (017–000–121; Jackson Immunoresearch Lab, MS) for 1h at room temperature, and then incubated with a primary antibody overnight at 4 °C. To illuminate the specific staining, a fluorescently labeled secondary antibody (Alexa-488 conjugated donkey-anti-rabbit or Alexa-594-conjugated donkey-antimouse) was applied (final 0.2μg/ml or diluted by 1:1000) for 2 h at room temperature. Rinsed sections were counterstained with DAPI and then mounted in Prolong Gold mounting medium (Invitrogen, Carlsbad, CA) and sealed under a cover slip. The primary and secondary antibodies are listed in Table S2. To visualize cones, sections were incubated with Fluorescein-labeled Peanut Agglutinin (PNA, Vector Laboratories, FL-1071, 1:500 dilution) for 1 h at room temperature and rinsed. Images were acquired under a 20× objective lens with a Nikon A1RS microscope. Immuno-fluorescence from central and mid-peripheral regions was quantified using ImageJ.

2.8. Photoaffinity labeling

Before S2R was cloned, photoaffinity labeling was essentially the only way to visualize S2R with a clear molecular size on a SDS gel [10,25]. The experiment was previously performed at University of Wisconsin-Madison, as described in our report [25]. Briefly, the neural retina was peeled off the mouse eyecup and RPE cells were gently dislodged and pipetted out, from which tissue homogenates and cell lysates were prepared. To detect specific S2R and S1R photolabeling, two aliquots (200 μg protein in each) of the same sample were pre-incubated without or with 20 μM 1,3-di-o-tolylguanidine (DTG, equal affinity for S2R and S1R) for 30 min at 32 °C in 50 mM Tris–HCL (pH 7.4) and 150 mM NaCl. The S2R/S1R-binding photoaffinity probe [^{125}I]-IAF (Iodoazido-fenpropimorf) was then added (final 1 nM) and incubated for another 40 min with gentle shaking in the dark. To photo-crosslink [^{125}I]-IAF to the proteins it binds, samples were exposed to a high-pressure AH-6 mercury lamp for 5 s followed by SDS-PAGE to separate proteins. Photo-labeled bands were visualized through autoradiography of dried SDS gel using Phosphoimager (Molecular Dynamics).

2.9. Illumination of reactive oxygen species (ROS)

The cell-permeable ROS-reactive fluorescent dye 2',7'-dichlorodihydrofluorescein diacetate (H_2DCFDA, Sigma-Aldrich, cat. D6883) was used. Once taken up by cells, the acetyl groups are cleaved off by intracellular esterases, resulting in H_2DCFH, which is oxidized by ROS and converted to the highly fluorescent molecule DCF [26]. ARPE19 cells (ATCC, CRL2302) were grown for 24 h in DMEM/F12 (ThermoFisher Scientific, cat#10565042) supplemented with 10% FBS in a 24-well plate, and treated with PBS or 5 mM $NaIO_3$ for various hours indicated in figure legends. To detect cellular ROS, the cells were changed to $NaIO_3$-free medium and incubated with 10 μM H_2DCFDA for 60 min at 37 °C prior to imaging [26]. The strong green fluorescence from DCF tended to saturate the detection channel. Therefore, to show a robust difference in ROS level between WT and TMEM97 KO cells, red fluorescence (Ex/m: 520/605 nm) was imaged for the 0–12 h time points of treatment with $NaIO_3$ and green fluorescence (Ex/m: 485/528 nm) was imaged for the 24 h time point, using an EVOS microscope (ThermoFisher Scientific). For ROS imaging *in vivo,* non-fixed retinal cryosections were incubated with 10μM H_2DCFDA for 60 min at 37 °C and imaged under the EVOS microscope.

2.10. Analysis of the mitochondrial membrane potential ($\Delta\Psi_M$)

We used an assay kit of 5,5,6,6'-tetrachloro-1,1',3,3' tetraethylbenzimi-dazoylcarbocyanine iodide (JC-1) from Biotium (Fremont, CA) following the manufacturer's instruction. JC-1 is a lipophilic, cationic dye which exhibits green fluorescence. After entering the negatively charged mitochondria with normal $\Delta\Psi_M$, the dye forms red fluorescent J-aggregates in a concentration-dependent manner [27]. ARPE19 cells were cultured to ~80% confluency and treated with 5 mM $NaIO_3$ for 3 h. At the end of treatment, cells were washed once with warm PBS (~37 °C) and incubated with the JC-1 (final 2 μM) working solution for 15 min in the cell culture incubator. The red or green fluorescence (Ex/m: 550/600 nm or 485/535 nm, respectively) intensity was measured by a TECAN Infinite 200Pro (Switzerland) spectrometry microplate reader. $\Delta\Psi_M$ is expressed as the intensity ratio of red *vs* green fluorescence.

2.11. Fluorescent detection of autophagosome-lysosome fusion via confocal microscopy

We followed the method as we recently reported [24] with minor modifications. We used an updated version of GFP-RFP-LC3 vector, namely, pHluorin (GFP variant)-mKate2 in tandem with human LC3 [28] (Addgene, #61460, product name FUGW-PK-hLC3). Briefly, cells were seeded onto glass-bottom dishes (NuncTM, 150680), stabilized for 24 h, and then transfected with the vector for 24 h. The cells were then treated with PBS or 5 mM $NaIO_3$ for 24 h and stained with 10 μM Hoechst 33342 (ThermoFisher, H3570) prior to live cell confocal microscopy. Images were acquired with a Nikon A1RS confocal microscope under a 40× oil objective lens.

2.12. TMEM97 KO single-clone ARPE19 cell lines

The generation of TMEM97 KO single-clone cell lines was performed using the same CRISPR/Cas9 genome-editing approach as we recently reported [29]. Briefly, one effective sgRNA sequence (5'-TCCGGCAACCAGGCGCTGCG –3') selected from 3 candidates (Table S3) was cloned into LentiCRISPR v2. Lentivirus was packaged and produced in HEK293FT cells (Invitrogen) with the second-generation packaging system, using pSPAX2 (Addgene, #12260) and pMD2.G (Addgene, #12259). ARPE19 cells (ATCC, CRL2302) were transduced with the lentivirus in DMEM/F12 supplemented with 10% FBS, at 37 °C under humidified conditions and 5% CO_2. The culture continued for 3 days, and then treated with 5 μg/ml puromycin for 2 weeks. Single clones were selected through serial dilutions and cultures. The cells transduced with the empty vector served as WT control.

2.13. TMEM97 overexpression ARPE19 cell lines

The cDNA of human *TMEM97* ORF was cloned from APRE19 cells, and subcloned into the pLenti-puro vector (Addgene, Cat#39481) in fusion with the V5 tag at the C terminus. The primers: TTCGGATC-CATGGGGGCTCCGGCAACCAG (forward);TTCGAATTCT-CATTTTTTTTTTCTTTTCTC (reverse). Lentivirus was produced as described above. Lentivirial titer was determined using Lenti-X GoStix Plus (TaKaRa) by measuring viral RNA content. ARPE19 cell transduction and single clone selection are described above. The selected clones were maintained in the DMEM/F12 medium supplemented with 10% FBS and 2 μg/ml puromycin.

2.14. Immunoblotting

The assay was performed as we previously reported [8]. Briefly, total protein amounts were quantified using DC Protein Assay Kit (Bio-Rad, Cat#5000111) and 50 μg per sample was loaded for SDS-PAGE. After transferring onto PVDF membrane, each specific protein was detected by using a primary antibody and a secondary antibody (listed in Table S2). Western blot images were recorded using Amersham Imager 680 (GE Healthcare) and processed with Image-J. Protein band densitometry was first normalized to loading control (GAPDH or β-actin) and then to the basal condition in each experiment (see the first bar in figures), and finally quantified as fold change. Fold changes from at least 3 independent experiments were averaged, and mean ± SEM was calculated.

2.15. Quantitative real time PCR (qRT-PCR)

Total RNA was extracted from cell lysates using TRIzol (ThermoFisher Scientific, cat#15596026) following the manufacturer's instructions. Purified mRNA (1 μg) was used for the first-strand cDNA synthesis and quantitative RT-PCR was performed using the Quant-Studio3 Real-Time PCR System (Applied Biosystems, Carlsbad, CA). Each cDNA template was amplified using SYBR Green PCR Master Mix. Primer sequences are provided in Table S4.

2.16. Statistical analysis

Prior to the analysis using GraphPad Prism, data sets were tested for normality using Shapiro–Wilk test. For two group comparison, Student's *t*-test was used. For multiple group comparisons, one-way analysis of variance (ANOVA) and *post hoc* test (specified in figure legends) was performed. Data are presented as mean ± standard error of the mean (SEM). Statistical significance was set as $*P < 0.05$.

3. Results

3.1. TMEM97 KO exacerbates retinal degeneration in an oxidant-induced mouse model

As shown in Fig. 1A (and Fig. S1), *via* immunostaining on healthy human retina sections, we were able to detect TMEM97 in the RPE layer. Moreover, through photoaffinity labeling, a sensitive pharmacology-based technique [10,25], S2R(TMEM97) was found to be expressed in both the RPE and neural retina (Fig. 1B). These results agree with the reported single-cell sequencing data indicative of the presence of TMEM97 transcripts in RPE/retinal cells [30]. To assess TMEM97's functional importance in oxidatively induced retinal degeneration, we administered sodium iodate ($NaIO_3$) intravenously to mice [31]. In WT mice, the outer nuclear layer (ONL, composed of photoreceptor cell bodies) became thinner 3 days after $NaIO_3$ injection. Interestingly, the ONL thickness was further reduced in TMEM97 KO mice compared to wild type controls (Fig. 2A and B, Fig. S2). In addition, consistent with RPE damage [32], $NaIO_3$-treated TMEM97 KO mice also exhibited intraretinal pigmented blebs (yellow arrows, Fig. 2B). Moreover, a fluorescent reactive oxygen species-sensitive probe revealed elevated ROS in TMEM97 KO compared to WT retinas during oxidative injury (Fig. 2C).

3.2. TMEM97 KO-induced retinal degeneration is attenuated by the antioxidant NAC

To explore potential contributors to the increase of ROS in the retinas of TMEM97 KO mice, we determine the expression of anti-oxidant enzymes in different pathways, including superoxide dismutases (SOD1, SOD2), catalase (CAT), and glutathione peroxidases (GPX1, GPX4). At 3 days after $NaIO_3$ injection, neuroretina and RPE were carefully extracted from the dissected eyecup. As shown in Fig. 3, the neuroretina showed minor levels of RPE65, a *bona fide* RPE marker which is minimally expressed in the neuroretina [33], suggesting clean preparation of the two different tissue samples. The mRNA level of mitochondrial superoxide dismutase (SOD2) was significantly lower in the KO (*vs* WT) RPE in the mice injected with PBS. A significant KO-*vs*-WT difference was not detected in the RPE of $NaIO_3$-treated mice (likely due to overall lowered mRNA after retinal damage), nor in the neuroretina of PBS- or $NaIO_3$-treated groups. SOD1 mRNA levels showed a very similar pattern of decrease in PBS-treated KO mice compared to controls, although it did not reach statistical significance. Similarly, there was a trend of reduced mRNA levels in the PBS-treated, but not $NaIO_3$-treated, KO *vs* WT RPE for other three anti-oxidant enzymes (without reaching statistical significance) and no change in the neuroretina. Overall, these results, in accordance with KO-induced retinal ROS surge (Fig. 2C), implicated an important role for TMEM97 against ROS elevation in the retina.

To further determine this novel role of TMEM97, we injected (i.p.) a commonly used antioxidant, *N*-acetyl cysteine (NAC) [34], following tail vein $NaIO_3$ injection in mice. Indeed, NAC significantly inhibited the ONL thickness loss mediated by $NaIO_3$ oxidative stress in TMEM97 KO mice (Fig. 4). In WT mice, NAC slightly increased (albeit non-significantly) the ONL thickness which was reduced by $NaIO_3$ treatment. Taken together, the results indicate that TMEM97 is a novel antioxidant player in the mouse retina/RPE.

3.3. TMEM97 KO exacerbates RPE cell oxidative stress and degenerative phenotype

In an *in vitro* model of oxidative damage, ROS levels induced by $NaIO_3$ dramatically increased in TMEM97 KO ARPE19 cells as compared to WT controls (Fig. 5A), as did the gene expression of ROS-producing enzymes [35] (Fig. S3). To determine the impact of TMEM97 KO on the development of a degenerative RPE cell phenotype, we measured active (cleaved) caspase-3, its substrate PARP1, and NFκB (p65, master pro-inflammatory transcription factor). In normal conditions (PBS control), these degenerative markers showed no significant changes between WT and TMEM97 KO (between a pair of black bars), whereas under $NaIO_3$ treatment they increased remarkably due to TMEM97 KO (comparison between a pair of red bars, Fig. 5B). We also measured DRP1, a key factor executing mitochondrial fragmentation which is often associated with apoptosis [36]. Consistently, DRP1 was markedly elevated during oxidative treatment in TMEM97 KO compared with WT controls (Fig. 5B). Further confirming the TMEM97 functional specificity, overexpression of TMEM97 diminished all 4 markers during oxidative stress (Fig. 5C), an effect opposite of TMEM97 KO during oxidative stress. Recent evidence indicates that certain degrees of mild oxidative stress can be protective by activating cytoprotective mechanisms such as antioxidant and autophagy pathways [1]. Our data appeared to be consistent, as $NaIO_3$ treatment reduced active caspase-3, NFκB, and DRP1

(Fig. 5) and increased NRF2 (Fig. 6) in WT cells, but not KO cells where ROS was substantially elevated.

3.4. TMEM97 KO down-regulates master antioxidant regulator NRF2 and its target gene product SOD2

We next measured the abundance of NRF2, the antioxidant master transcription factor, and SOD2, a *bona fide* downstream product of NRF2 transcriptional activity. Abundance of both proteins was reduced in TMEM97 KO cells, either with or without $NaIO_3$ treatment (Fig. 6A/B). The difference in NRF2 abundance between WT and KO cells was not abolished by NAC (ROS quencher) (Fig. 6C). We also determined the levels of POLDIP2 which is a recently identified mitochondrial protein associated with ROS elevation [37], and TOM20, a mitochondrial membrane protein whose accumulation is often used to monitor impaired autophagic clearance of damaged mitochondria [38]. Interestingly, abundance of both proteins was increased in TMEM97 KO cells with or without $NaIO_3$-treatment (Fig. 6A/B). qRT-PCR revealed that *SOD2* mRNA was diminished by TMEM97 loss and increased by TMEM97 overexpression (Fig. 6D), consistent with *SOD2* being a NRF2 target gene. Changes were insignificant or minor in *NRF2* and *POLDIP2* mRNA levels, suggesting that TMEM97 ablation mainly affected their protein levels rather than mRNA expression.

3.5. TMEM97 KO affects mitochondrial and lysosomal stability

In addition to the impact on the SOD2, POLDIP2, and DRP1 proteins involved in mitochondrial functions, the mitochondrial membrane potential ($\Delta\Psi_M$) was lower in TMEM97 KO (*vs* WT) cells, as revealed by JC-1 assay (Fig. 6E), in which a reduced red-*vs*-green fluorescence intensity ratio reflects mitochondrial membrane depolarization [27]. Moreover, TOM20 which, along with damaged mitochondria, is typically removed through lysosome-mediated mitophagy [39], instead accumulated in KO cells (Fig. 6A/B), implicating lysosomal malfunction. Indeed, TMEM97 loss- and gain-of-function, respectively, reduced and increased ATP6V0D1 (Fig. 7A), which is a subunit key to the proton pump activity of v(vacuolar)-ATPase, the multi-subunit complex enabling lysosomal acidification and hence proteolytic function [40]. Consistently, lysosomal protease cathepsin-D was markedly lower, and the lysosome-mediated turnover of LC3II and p62 (markers of autophagosome cargo) was impaired in KO compared with WT cells (Fig. 7B). Moreover, TMEM97 KO ARPE19 cells showed evidence of compromised lysosomal function under $NaIO_3$ treatment, as measured by the pHluorin-mKate2-hLC3 reporter vector [28] (Fig. 7C, Fig. S4). A recent study reported that dysfunctional lysosomes in normoxic conditions raised levels of the HIF1α protein, the master hypoxia response factor [40]. Interestingly, we also observed elevated HIF1α protein (but not mRNA) in $NaIO_3$-treated TMEM97 KO cells compared to WT cells (Fig. 7D), in line with lysosomal dysfunction. On the other hand, the total mass of lysosomes was unaltered, as indicated by no change in LAMP1 and LAMP2 levels (Fig. S5).

4. Discussion

The major finding of this study is that TMEM97 ablation aggravates oxidant-induced retinal degeneration. Specifically, in TMEM97 KO *vs* WT mice, retinal ROS and photoreceptor

loss were both heightened under $NaIO_3$-induced oxidative stress. Consistently, in oxidant-stressed ARPE19 cells, TMEM97 KO increased ROS levels and promoted an RPE degenerative phenotype. Further analyses revealed that TMEM97 KO not only reduced the antioxidant master transcription factor NRF2 but also disturbed mitochondria, lysosomes, and autophagy flux - all subcellular systems important for redox homeostasis [1,23]. These results together suggest that TMEM97 is a previously uncharacterized multifunctional modulator of redox balancing processes.

To the best of our knowledge, this is the first report of TMEM97 countering oxidant-induced retinal degeneration. Our finding is pathophysiologically relevant. First, using different methods, we detected an abundance of TMEM97 protein in both mouse and human RPE. Second, our finding was based on a well-characterized *in vivo* oxidative stress model, whereby $NaIO_3$ induces retinal degeneration by initially damaging the RPE [19–21]. Third, the $NaIO_3$ dose we used was well within the range that does not cause systemic toxicity in pharmacokinetics studies in mice [41]. Moreover, echoing our finding, recent GWAS and TWAS studies discovered several putative new risk loci associated with AMD, including *TMEM97*, implicating its potential importance in the retina and RPE [5,6,30]. Without follow-up functional studies available, it is unclear whether the *TMEM97* variant could truly impact retinal degeneration, and it remains an interesting question whether the *TMEM97* SNP (rs11080055) [5] could have a similar functional impact in the RPE as the TMEM97 KO observed here. Taken together, our study suggests that TMEM97 could play an important role in the RPE by mitigating oxidative damage, although a definitive elucidation of this role will require future studies using, for example, RPE-specific TMEM97 KO mice. Nevertheless, we observed marked damage in the RPE layer following oxidant treatment of TMEM97 KO mice. In addition, we found dramatic increases of ROS and degenerative phenotype markers in KO (*vs* WT) ARPE19 cells under $NaIO_3$ treatment. These results offer *in vitro* evidence of RPE-specific TMEM97 function against oxidative damage. In accordance with our finding of an antioxidant function of TMEM97, the Bowen lab showed that a S2R agonist reduced ROS, albeit in a different context using a cancer cell line [42]. Much research is needed to reconcile sometimes contradicting results from pharmacologic and genetic studies, especially considering recently revealed TMEM97-independent S2R ligand activities [18].

NRF2 is a master transcription factor that governs an antioxidant response system comprised of around one hundred genes [43]. In this light, our novel finding of TMEM97 regulation of NRF2 protein levels is significant. Cytosolic NRF2 is bound with KEAP1 which promotes NRF2 ubiquitination [1]. NRF2 is constantly degraded due to this association until disrupted by ROS oxidation of KEAP1. Since ROS as a signal elevate NRF2, down-regulation of NRF2 in TMEM97 KO cells observed herein does not appear to be a secondary event of KO-caused ROS surge. In fact, in the presence of an ROS quencher (NAC), NRF2 still decreased in KO (*vs* WT) cells. Binding of KEAP1 by other proteins such as p62 (SQSTM1), a key factor in autophagy flux, can also stabilize NRF2 [1]. This may not account for the impact of TMEM97 KO on NRF2 either, since no significant change in p62 occurred in KO *vs* WT cells. Interestingly, the Smith group reported an important role of S1R in regulating NRF2 [43]. However, caution should be taken in correlating results derived from S1R and TMEM97(S2R), as these two differ not only in their coding genes but

also functions [44,45]. Since our data showed that TMEM97 ablation led to reduced NRF2 protein but not mRNA, the next logic step would be to explore whether NRF2 ubiquitination and proteasomal degradation account for the observed NRF2 protein level change. Thus, the TMEM97 molecular action underlying its regulation of NRF2 stability represents an intriguing research direction that warrants further investigation.

Beyond the regulation of NRF2, the negative impact of TMEM97 KO on organelle stability is another new finding. While metabolically active mitochondria maintain cellular bioenergetics, lysosomes recycle cellular wastes [39]. Dysfunction of these organelles, which culminates in dysregulated autophagy flux, heightens oxidative stress [23]. In fact, these endogenous redox-balancing systems, namely, NRF2, mitochondria, lysosomes, and autophagy, constitute a network *via* their interplay [46], as also implicated in our results. For instance, the mitochondrion-residing superoxide dismutase (SOD2) is encoded by NRF2's target gene. Indeed, the changes of SOD2 protein (and also mRNA) levels mirrored that of NRF2 protein in response to oxidant treatment and/or TMEM97 KO. POLDIP2 is a recently identified redox regulator found in mitochondria as well [38]. The POLDIP2/NOX4 axis was reported to elicit oxidative mitochondrial damage [47]. The portions of damaged mitochondria are typically removed through DRP1-assisted fission and mitophagy directed to recycling in lysosomes. Consistently, DRP1 which can augment mitochondrial dysfunction [36], was herein found upregulated due to TMEM97 KO, a change opposite to that of NRF2. This result concurs with a recent report of a novel regulation whereby NRF2 promotes DRP1 degradation [48]. Though traditionally viewed as merely a “garbage bag”, the lysosome is increasingly recognized as a signaling hub [40,49]. Moreover, dysfunctional lysosomes leak ROS into the cytosol [49]. Interestingly, a very recent study found that lysosomal dysfunction due to v-ATPase instability manifested aberrant normoxic increase of HIF1α protein, the master hypoxic response factor [40]. Herein we also observed a significant increase of HIF1α under non-hypoxic conditions in oxidatively stressed TMEM97 KO cells *vs* WT controls. Moreover, it is known that heightened HIF1α activity inhibits mitochondrial function, hereby linking dysfunctional lysosomes to mitochondrial dysregulation [40]. Importantly, suggestive of lysosomal dysfunction, TMEM97 KO reduced levels of ATP6V0D1, a key subunit in the v-ATPase assembly. Destabilized v-ATPase is known to jeopardize lysosomal protease stability [40], as also exemplified by our observation of decreased cathepsin-D in TMEM97 KO *vs* WT cells. Reduced lysosomal proteolytic capacity inevitably impairs autophagic cargo digestion [50]. Indeed, we observed impeded turnover of LC3II and p62 as well as TOM20 (a marker of mitophagy cargo) due to TMEM97 KO. Taken together, TMEM97 appears to play an important role in regulating not only NRF2 stability but also organelle homeostasis in oxidatively stressed ARPE19 cells. The molecular details of these regulations await future elucidation (see a hypothetical working model in Fig. 8). Nonetheless, the functional importance of TMEM97 that manifests under oxidative stress could be rationalized by its broad subcellular distribution (and redistribution) in the endoplasmic reticulum, lysosome, and plasma membranes [7].

5. Conclusion

TMEM97 ablation exacerbates retinal degeneration in an oxidant-induced mouse model, and complementary *in vitro* results suggest that TMEM97 regulates NRF2 as well as organelle

stability in oxidatively stressed ARPE19 cells. Further studies may help evaluate TMEM97 as a potential interventional target against retinal degeneration or beyond, especially in view of recent advances in clinical trials of S2R ligands for Alzheimer's, Schizophrenia, and COVID-19 [13,15,51].

Supplementary Material

Refer to Web version on PubMed Central for supplementary material.

Acknowledgments and sources of funding

Dr. Guo has received support from NIH R01 grant EY029809. Dr. Gelfand has received support from NIH grants (R01EY028027 and R01EY031039), BrightFocus Foundation, and the Owens Family Foundation. Dr. Cebulla holds the Torrence A. Makley Research Professorship and receives support from the Ohio Lions Eye Research Foundation. We thank Dr. Arnold E Ruoho for his support with the photoaffinity labeling reagents and equipment.

References

[1]. Datta S, Cano M, Ebrahimi K, Wang L, Handa JT, The impact of oxidative stress and inflammation on RPE degeneration in non-neovascular AMD, Prog. Retin. Eye Res. 60 (2017) 201–218. [PubMed: 28336424]

[2]. Elbatreek MH, Mucke H, Schmidt H, NOX inhibitors: from bench to Naxibs to bedside, Handb. Exp. Pharmacol. 264 (2021) 145–168. [PubMed: 32780287]

[3]. Xu L, Kong L, Wang J, Ash JD, Stimulation of AMPK prevents degeneration of photoreceptors and the retinal pigment epithelium, Proc. Natl. Acad. Sci. U. S. A. 115 (2018) 10475–10480. [PubMed: 30249643]

[4]. Felszeghy S, Viiri J, Paterno JJ, Hyttinen JMT, Koskela A, Chen M, Leinonen H, Tanila H, Kivinen N, Koistinen A, Toropainen E, Amadio M, Smedowski A, Reinisalo M, Winiarczyk M, Mackiewicz J, Mutikainen M, Ruotsalainen AK, Kettunen M, Jokivarsi K, Sinha D, Kinnunen K, Petrovski G, Blasiak J, Bjorkoy G, Koskelainen A, Skottman H, Urtti A, Salminen A, Kannan R, Ferrington DA, Xu H, Levonen AL, Tavi P, Kauppinen A, Kaarniranta K, Loss of NRF-2 and PGC-1alpha genes leads to retinal pigment epithelium damage resembling dry age-related macular degeneration, Redox Biol. 20 (2019) 1–12. [PubMed: 30253279]

[5]. Ratnapriya R, Sosina OA, Starostik MR, Kwicklis M, Kapphahn RJ, Fritsche LG, Walton A, Arvanitis M, Gieser L, Pietraszkiewicz A, Montezuma SR, Chew EY, Battle A, Abecasis GR, Ferrington DA, Chatterjee N, Swaroop A, Retinal transcriptome and eQTL analyses identify genes associated with age-related macular degeneration, Nat. Genet. 51 (2019) 606–610. [PubMed: 30742112]

[6]. Fritsche LG, Igl W, Bailey JN, Grassmann F, Sengupta S, Bragg-Gresham JL, Burdon KP, Hebbring SJ, Wen C, Gorski M, Kim IK, Cho D, Zack D, Souied E, Scholl HP, Bala E, Lee KE, Hunter DJ, Sardell RJ, Mitchell P, Merriam JE, Cipriani V, Hoffman JD, Schick T, Lechanteur YT, Guymer RH, Johnson MP, Jiang Y, Stanton CM, Buitendijk GH, Zhan X, Kwong AM, Boleda A, Brooks M, Gieser L, Ratnapriya R, Branham KE, Foerster JR, Heckenlively JR, Othman MI, Vote BJ, Liang HH, Souzeau E, McAllister IL, Isaacs T, Hall J, Lake S, Mackey DA, Constable IJ, Craig JE, Kitchner TE, Yang Z, Su Z, Luo H, Chen D, Ouyang H, Flagg K, Lin D, Mao G, Ferreyra H, Stark K, von Strachwitz CN, Wolf A, Brandl C, Rudolph G, Olden M, Morrison MA, Morgan DJ, Schu M, Ahn J, Silvestri G, Tsironi EE, Park KH, Farrer LA, Orlin A, Brucker A, Li M, Curcio CA, Mohand-Said S, Sahel JA, Audo I, Benchaboune M, Cree AJ, Rennie CA, Goverdhan SV, Grunin M, Hagbi-Levi S, Campochiaro P, Katsanis N, Holz FG, Blond F, Blanche H, Deleuze JF, Igo RP Jr, Truitt B, Peachey NS, Meuer SM, Myers CE, Moore EL, Klein R, Hauser MA, Postel EA, Courtenay MD, Schwartz SG, Kovach JL, Scott WK, Liew G, Tan AG, Gopinath B, Merriam JC, Smith RT, Khan JC, Shahid H, Moore AT, McGrath JA, Laux R, Brantley MA Jr., Agarwal A, Ersoy L, Caramoy A, Langmann T, Saksens NT, de Jong EK, Hoyng CB, Cain MS, Richardson AJ, Martin TM, Blangero J, Weeks DE, Dhillon B, van Duijn CM, Doheny KF, Romm J, Klaver CC, Hayward C, Gorin MB, Klein ML, Baird

PN, den Hollander AI, Fauser S, Yates JR, Allikmets R, Wang JJ, Schaumberg DA, Klein BE, Hagstrom SA, Chowers I, Lotery AJ, Leveillard T, Zhang K, Brilliant MH, Hewitt AW, Swaroop A, Chew EY, Pericak-Vance MA, DeAngelis M, Stambolian D, Haines JL, Iyengar SK, Weber BH, Abecasis GR, Heid IM, A large genome-wide association study of age-related macular degeneration highlights contributions of rare and common variants, Nat. Genet. 48 (2016) 134–143. [PubMed: 26691988]

[7]. Bartz F, Kern L, Erz D, Zhu M, Gilbert D, Meinhof T, Wirkner U, Erfle H, Muckenthaler M, Pepperkok R, Runz H, Identification of cholesterol-regulating genes by targeted RNAi screening, Cell Metab. 10 (2009) 63–75. [PubMed: 19583955]

[8]. Shen H, Li J, Xie X, Yang H, Zhang M, Wang B, Kent KC, Plutzky J, Guo LW, BRD2 regulation of sigma-2 receptor upon cholesterol deprivation, Life Sci Alliance. 4 (2021).

[9]. Riad A, Lengyel-Zhand Z, Zeng C, Weng CC, Lee VM, Trojanowski JQ, Mach RH, The Sigma-2 Receptor/TMEM97, PGRMC1, and LDL receptor complex are responsible for the cellular uptake of Abeta42 and its protein aggregates, Mol. Neurobiol. 57 (2020) 3803–3813. [PubMed: 32572762]

[10]. Hellewell SB, Bowen WD, A sigma-like binding site in rat pheochromocytoma (PC12) cells: decreased affinity for ()-benzomorphans and lower molecular weight suggest a different sigma receptor form from that of Guinea pig brain, Brain Res. 527 (1990) 244–253. [PubMed: 2174717]

[11]. Matsumoto RR, Nguyen L, Kaushal N, Robson MJ, Sigma (sigma) receptors as potential therapeutic targets to mitigate psychostimulant effects, Adv. Pharmacol. 69 (2014) 323–386. [PubMed: 24484982]

[12]. Alon A, Schmidt HR, Wood MD, Sahn JJ, Martin SF, Kruse AC, Identification of the gene that codes for the sigma2 receptor, Proc. Natl. Acad. Sci. U. S. A. 114 (2017) 7160–7165. [PubMed: 28559337]

[13]. Grundman M, Morgan R, Lickliter JD, Schneider LS, DeKosky S, Izzo NJ, Guttendorf R, Higgin M, Pribyl J, Mozzoni K, Safferstein H, Catalano SM, A phase 1 clinical trial of the sigma-2 receptor complex allosteric antagonist CT1812, a novel therapeutic candidate for Alzheimer's disease, Alzheimers Dement. (N Y). 5 (2019) 20–26. [PubMed: 30723776]

[14]. Blass BE, Rogers JP, The sigma-2 (sigma-2) receptor: a review of recent patent applications: 2013–2018, Expert Opin. Ther. Pat. 28 (2018) 655–663. [PubMed: 30185082]

[15]. Davidson M, Saoud J, Staner C, Noel N, Luthringer E, Werner S, Reilly J, Schaffhauser JY, Rabinowitz J, Weiser M, Luthringer R, Efficacy and safety of MIN-101: a 12-week randomized, double-blind, placebo-controlled trial of a new drug in development for the treatment of negative symptoms in schizophrenia, Am. J. Psychiatry 174 (2017) 1195–1202. [PubMed: 28750582]

[16]. Gordon DE, Jang GM, Bouhaddou M, Xu J, Obernier K, White KM, O'Meara MJ, Rezelj VV, Guo JZ, Swaney DL, Tummino TA, Huttenhain R, Kaake RM, Richards AL, Tutuncuoglu B, Foussard H, Batra J, Haas K, Modak M, Kim M, Haas P, Polacco BJ, Braberg H, Fabius JM, Eckhardt M, Soucheray M, Bennett MJ, Cakir M, McGregor MJ, Li Q, Meyer B, Roesch F, Vallet T, Mac Kain A, Miorin L, Moreno E, Naing ZZC, Zhou Y, Peng S, Shi Y, Zhang Z, Shen W, Kirby IT, Melnyk JE, Chorba JS, Lou K, Dai SA, Barrio-Hernandez I, Memon D, Hernandez-Armenta C, Lyu J, Mathy CJP, Perica T, Pilla KB, Ganesan SJ, Saltzberg DJ, Rakesh R, Liu X, Rosenthal SB, Calviello L, Venkataramanan S, Liboy-Lugo J, Lin Y, Huang XP, Liu Y, Wankowicz SA, Bohn M, Safari M, Ugur FS, Koh C, Savar NS, Tran QD, Shengjuler D, Fletcher SJ, O'Neal MC, Cai Y, Chang JCJ, Broadhurst DJ, Klippsten S, Sharp PP, Wenzell NA, Kuzuoglu-Ozturk D, Wang HY, Trenker R, Young JM, Cavero DA, Hiatt J, Roth TL, Rathore U, Subramanian A, Noack J, Hubert M, Stroud RM, Frankel AD, Rosenberg OS, Verba KA, Agard DA, Ott M, Emerman M, Jura N, von Zastrow M, Verdin E, Ashworth A, Schwartz O, d'Enfert C, Mukherjee S, Jacobson M, Malik HS, Fujimori DG, Ideker T, Craik CS, Floor SN, Fraser JS, Gross JD, Sali A, Roth BL, Ruggero D, Taunton J, Kortemme T, Beltrao P, Vignuzzi M, Garcia-Sastre A, Shokat KM, Shoichet BK, Krogan NJ, A SARS-CoV-2 protein interaction map reveals targets for drug repurposing, Nature 583 (2020) 459–468. [PubMed: 32353859]

[17]. Liu X, Fu Y, Yang H, Mavlyutov T, Li J, McCurdy CR, Guo LW, Pattnaik BR, Potential independent action of sigma receptor ligands through inhibition of the Kv2.1 channel, Oncotarget 8 (2017) 59345–59358. [PubMed: 28938641]

[18]. Zeng C, Weng CC, Schneider ME Jr., Puentes L, Riad A, Xu K, Makvandi M, Jin L, Hawkins WG, Mach RH, TMEM97 and PGRMC1 do not mediate sigma-2 ligand-induced cell death, Cell Death Discov. 5 (2019) 58. [PubMed: 30701090]

[19]. Sreekumar PG, Li Z, Wang W, Spee C, Hinton DR, Kannan R, MacKay JA, Intra-vitreal alphaB crystallin fused to elastin-like polypeptide provides neuroprotection in a mouse model of age-related macular degeneration, J. Control. Rel. 283 (2018) 94–104.

[20]. Franco LM, Zulliger R, Wolf-Schnurrbusch UE, Katagiri Y, Kaplan HJ, Wolf S, Enzmann V, Decreased visual function after patchy loss of retinal pigment epithelium induced by low-dose sodium iodate, Invest. Ophthalmol. Vis. Sci. 50 (2009) 4004–4010. [PubMed: 19339739]

[21]. Upadhyay M, Milliner C, Bell BA, Bonilha VL, Oxidative stress in the retina and retinal pigment epithelium (RPE): role of aging, and DJ-1, Redox Biol. (2020) 101623. [PubMed: 32826201]

[22]. Chen C, Cano M, Wang JJ, Li J, Huang C, Yu Q, Herbert TP, Handa JT, Zhang SX, Role of unfolded protein response dysregulation in oxidative injury of retinal pigment epithelial cells, Antioxid. Redox Signal. 20 (2014) 2091–2106. [PubMed: 24053669]

[23]. Mitter SK, Song C, Qi X, Mao H, Rao H, Akin D, Lewin A, Grant M, Dunn W Jr., Ding J, Bowes C. Rickman, Boulton M, Dysregulated autophagy in the RPE is associated with increased susceptibility to oxidative stress and AMD, Autophagy 10 (2014) 1989–2005. [PubMed: 25484094]

[24]. Yang H, Fu Y, Liu X, Shahi PK, Mavlyutov TA, Li J, Yao A, Guo SZ, Pattnaik BR, Guo LW, Role of the sigma-1 receptor chaperone in rod and cone photoreceptor degenerations in a mouse model of retinitis pigmentosa, Mol. Neurodegener. 12 (2017) 68. [PubMed: 28927431]

[25]. Chu UB, Mavlyutov TA, Chu ML, Yang H, Schulman A, Mesangeau C, McCurdy CR, Guo LW, Ruoho AE, The Sigma-2 receptor and progesterone receptor membrane component 1 are different binding sites derived from independent genes, EBioMedicine. 2 (2015) 1806–1813. [PubMed: 26870805]

[26]. Kim H, Xue X, Detection of total reactive oxygen species in adherent cells by 2',7'-dichlorodihydrofluorescein diacetate staining, J. Vis. Exp. 160 (2020), 10.3791/60682.

[27]. Sivandzade F, Bhalerao A, Cucullo L, Analysis of the mitochondrial membrane potential using the cationic JC-1 dye as a sensitive fluorescent probe, Bio Protoc. 9 (2019).

[28]. Tanida I, Ueno T, Uchiyama Y, A super-ecliptic, pHluorin-mKate2, tandem fluorescent protein-tagged human LC3 for the monitoring of mammalian autophagy, PLoS One. 9 (2014), e110600. [PubMed: 25340751]

[29]. Yang H, Shen H, Li J, Guo LW, SIGMAR1/Sigma-1 receptor ablation impairs autophagosome clearance, Autophagy 15 (2019) 1539–1557. [PubMed: 30871407]

[30]. Orozco LD, Chen HH, Cox C, Katschke KJ Jr., Arceo R, Espiritu C, Caplazi P, Nghiem SS, Chen YJ, Modrusan Z, Dressen A, Goldstein LD, Clarke C, Bhangale T, Yaspan B, Jeanne M, Townsend MJ, Campagne M. van Lookeren J., Hackney A, Integration of eQTL and a single-cell atlas in the human eye identifies causal genes for age-related macular degeneration, Cell Rep. 30 (1246–1259) (2020), e6.

[31]. Wang J, Iacovelli J, Spencer C, Saint-Geniez M, Direct effect of sodium iodate on neurosensory retina, Invest. Ophthalmol. Vis. Sci. 55 (2014) 1941–1953. [PubMed: 24481259]

[32]. Zanzottera EC, Messinger JD, Ach T, Smith RT, Freund KB, Curcio CA, The project MACULA retinal pigment epithelium grading system for histology and optical coherence tomography in age-related macular degeneration, Invest. Ophthalmol. Vis. Sci. 56 (2015) 3253–3268. [PubMed: 25813989]

[33]. Znoiko SL, Crouch RK, Moiseyev G, Ma JX, Identification of the RPE65 protein in mammalian cone photoreceptors, Invest. Ophthalmol. Vis. Sci. 43 (2002) 1604–1609. [PubMed: 11980880]

[34]. Sano H, Namekata K, Kimura A, Shitara H, Guo X, Harada C, Mitamura Y, Harada T, Differential effects of N-acetylcysteine on retinal degeneration in two mouse models of normal tension glaucoma, Cell Death Dis. 10 (2019) 75. [PubMed: 30692515]

[35]. Berencsi K, Bakay M, Beladi I, The role of macrophages in adenovirus-induced immunosuppression in mice, Acta Virol. 29 (1985) 61–65. [PubMed: 2859763]

[36]. Haileselassie B, Joshi AU, Minhas PS, Mukherjee R, Andreasson KI, Mochly-Rosen D, Mitochondrial dysfunction mediated through dynamin-related protein 1 (Drp1) propagates

impairment in blood brain barrier in septic encephalopathy, J. Neuroinflammation 17 (2020) 36. [PubMed: 31987040]

[37]. Lyle AN, Deshpande NN, Taniyama Y, Seidel-Rogol B, Pounkova L, Du P, Papaharalambus C, Lassegue B, Griendling KK, Poldip2, a novel regulator of Nox4 and cytoskeletal integrity in vascular smooth muscle cells, Circ. Res. 105 (2009) 249–259. [PubMed: 19574552]

[38]. Paredes F, Sheldon K, Lassegue B, Williams HC, Faidley EA, Benavides GA, Torres G, Sanhueza-Olivares F, Yeligar SM, Griendling KK, Darley-Usmar V, Martin A San, Poldip2 is an oxygen-sensitive protein that controls PDH and alphaKGDH lipoylation and activation to support metabolic adaptation in hypoxia and cancer, Proc. Natl. Acad. Sci. U. S. A. 115 (2018) 1789–1794. [PubMed: 29434038]

[39]. Plotegher N, Duchen MR, Mitochondrial dysfunction and neurodegeneration in lysosomal storage disorders, Trends Mol. Med. 23 (2017) 116–134. [PubMed: 28111024]

[40]. Miles AL, Burr SP, Grice GL, Nathan JA, The vacuolar-ATPase complex and assembly factors, TMEM199 and CCDC115, control HIF1alpha prolyl hydroxylation by regulating cellular iron levels, elife 6 (2017).

[41]. Chowers G, Cohen M, Marks-Ohana D, Stika S, Eijzenberg A, Banin E, Obolensky A, Course of sodium iodate-induced retinal degeneration in albino and pigmented mice, Invest. Ophthalmol. Vis. Sci. 58 (2017) 2239–2249. [PubMed: 28418497]

[42]. Nicholson H, Mesangeau C, McCurdy CR, Bowen WD, Sigma-2 receptors play a role in cellular metabolism: stimulation of glycolytic hallmarks by CM764 in human SK-N-SH neuroblastoma, J. Pharmacol. Exp. Ther. 356 (2016) 232–243. [PubMed: 26574517]

[43]. Wang J, Shanmugam A, Markand S, Zorrilla E, Ganapathy V, Smith SB, Sigma 1 receptor regulates the oxidative stress response in primary retinal muller glial cells via NRF2 signaling and system xc(-), the Na()-independent glutamate-cystine exchanger, Free Radic. Biol. Med. 86 (2015) 25–36. [PubMed: 25920363]

[44]. Sanchez-Blazquez P, Cortes-Montero E, Rodriguez-Munoz M, Merlos M, Garzon-Nino J, The Sigma 2 receptor promotes and the Sigma 1 receptor inhibits mu-opioid receptor-mediated antinociception, Mol. Brain. 13 (2020) 150. [PubMed: 33176836]

[45]. Aydar E, Cobos EJ, Maurice T, Murell-Lagnado RD, Safrany ST, Editorial: sigma receptors, Front. Pharmacol. 11 (2020), 590519. [PubMed: 33013426]

[46]. Handa JT, Bowes Rickman C, Dick AD, Gorin MB, Miller JW, Toth CA, Ueffing M, Zarbin M, Farrer LA, A systems biology approach towards understanding and treating non-neovascular age-related macular degeneration, Nat. Commun. 10 (2019) 3347. [PubMed: 31350409]

[47]. Li L, Lai EY, Luo Z, Solis G, Mendonca M, Griendling KK, Wellstein A, Welch WJ, Wilcox CS, High salt enhances reactive oxygen species and angiotensin II contractions of glomerular afferent arterioles from mice with reduced renal mass, Hypertension 72 (2018) 1208–1216. [PubMed: 30354808]

[48]. Sabouny R, Fraunberger E, Geoffrion M, Ng AC, Baird SD, Screaton RA, Milne R, McBride HM, Shutt TE, The Keap1-Nrf2 stress response pathway promotes mitochondrial hyperfusion through degradation of the mitochondrial fission protein Drp1, Antioxid. Redox Signal. 27 (2017) 1447–1459. [PubMed: 28494652]

[49]. Wang F, Gomez-Sintes R, Boya P, Lysosomal membrane permeabilization and cell death, Traffic 19 (2018) 918–931. [PubMed: 30125440]

[50]. Leeman DS, Hebestreit K, Ruetz T, Webb AE, McKay A, Pollina EA, Dulken BW, Zhao X, Yeo RW, Ho TT, Mahmoudi S, Devarajan K, Passegue E, Rando TA, Frydman J, Brunet A, Lysosome activation clears aggregates and enhances quiescent neural stem cell activation during aging, Science 359 (2018) 1277–1283. [PubMed: 29590078]

[51]. Abate C, Niso M, Abatematteo FS, Contino M, Colabufo NA, Berardi F, PB28, the Sigma-1 and Sigma-2 receptors modulator with potent anti-SARS-CoV-2 activity: a review about its pharmacological properties and structure affinity relationships, Front. Pharmacol. 11 (2020), 589810. [PubMed: 33364961]

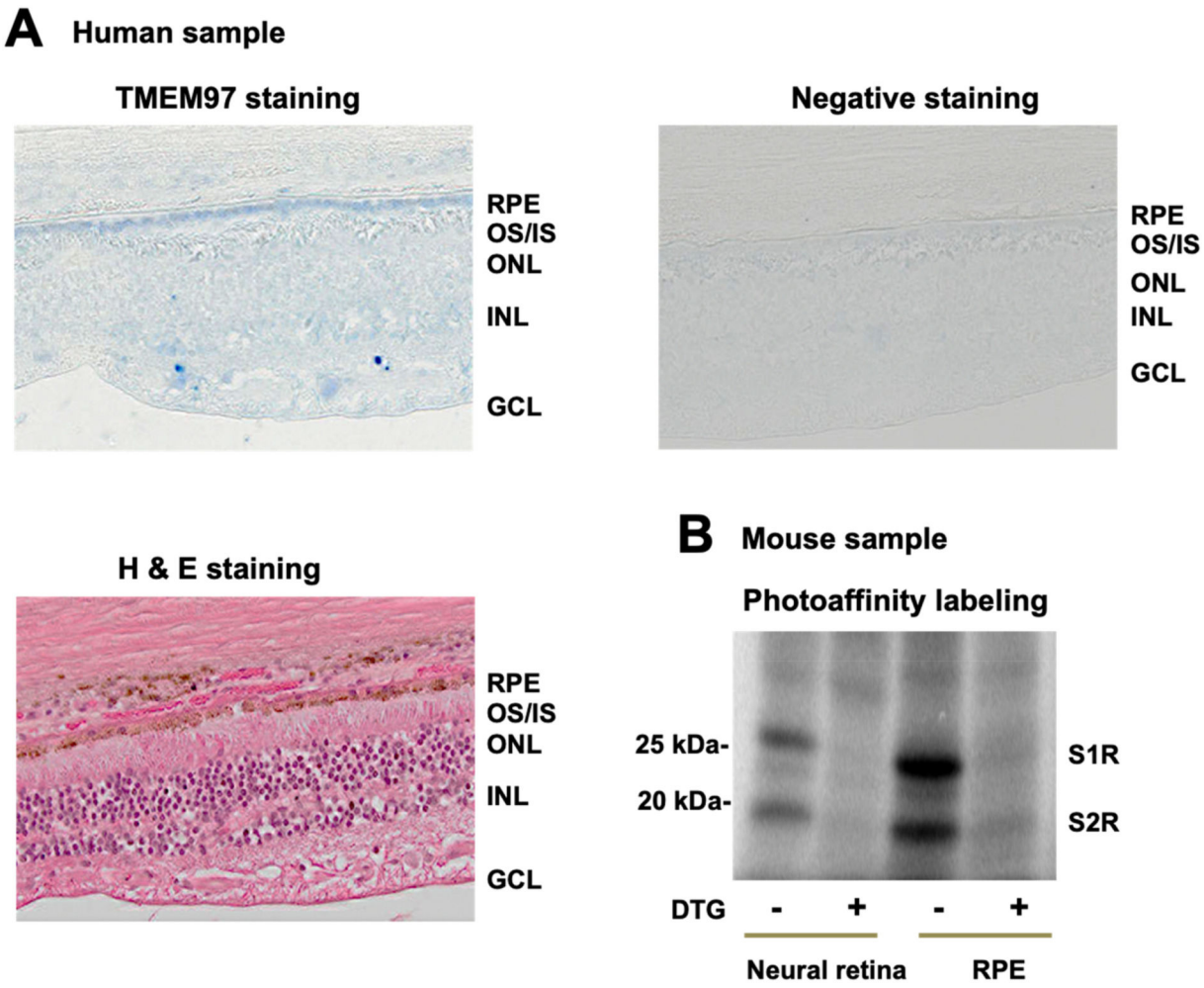

Fig. 1. Detection of TMEM97 in human and mouse RPE and neural retina tissues.

A. Immunostaining of TMEM97 on human retinal sections. To minimize the interference of the pigmented background (see the brownish color in the RPE layer of H&*E*-stained section), the pigments were bleached, and immunohistochemistry rather than immunofluorescence (autofluorescence is high) was performed using an alkaline phosphatase-conjugated secondary antibody. RPE: retinal pigment epithelium. OS/IS: Photoreceptor outer and inner segments. ONL/INL: Outer and inner nuclear layer. GCL: Ganglion cell layer.

B. Photoaffinity labeling of mouse TMEM97(S2R). Neural retinal tissues and RPE cells were isolated as described in Methods. DTG is a ligand selective for both sigma-1 receptor (S1R) and S2R (TMEM97) with equal affinity. Thus, photolabeling blockage (bands disappearing) by DTG as a competitor of the radiolabeled photoaffinity ligand indicates photolabeling specificity for TMEM97 and S1R.

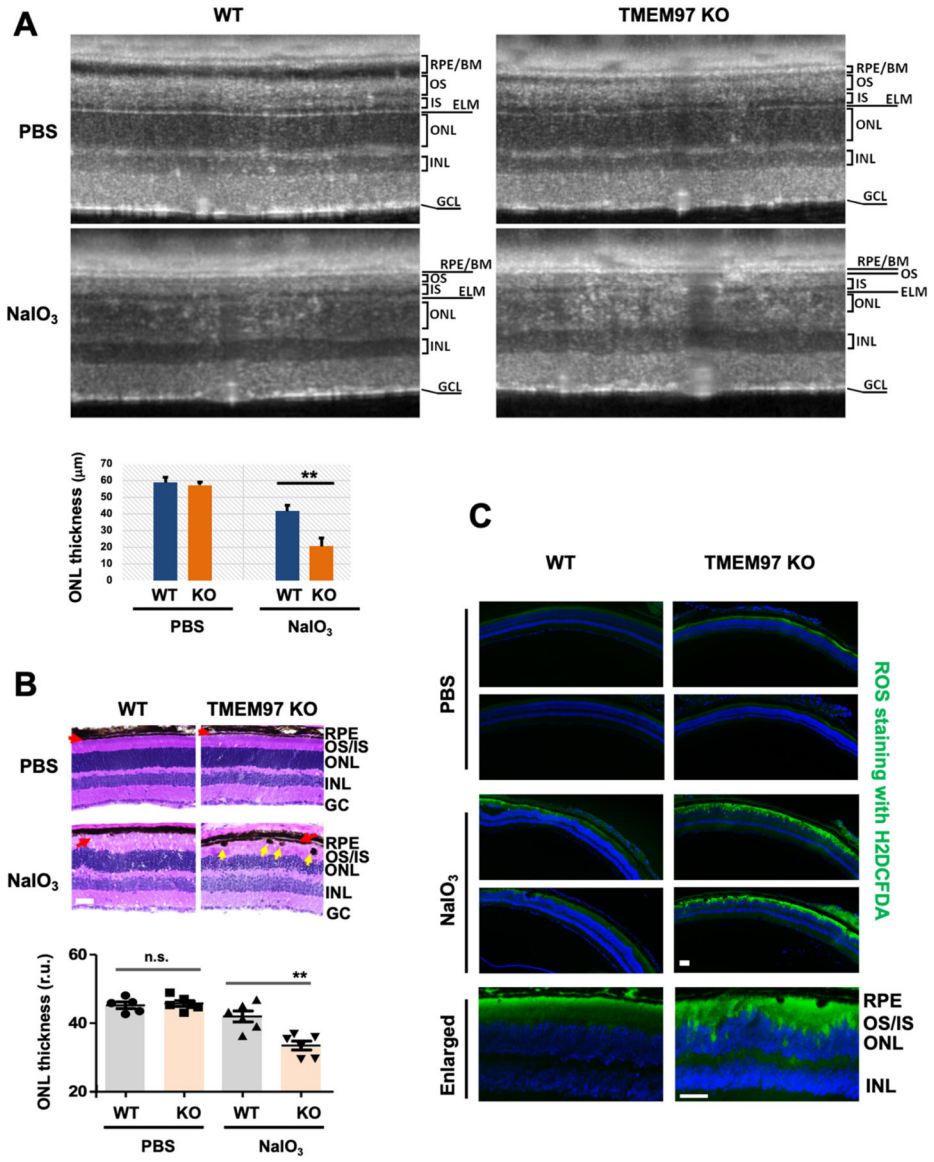

Fig. 2. Exacerbated retinal degeneration in TMEM97 KO mice.

A. Exacerbated photoreceptor loss in KO *vs* WT retinas (SD-OCT imaging). Live animal imaging was performed on PBS control mice and $NaIO_3$-treated mice on day 3 post injection. Retinal (ONL) thickness was measured with the Bioptigen InVivoVue Diver software using manual marker placement and auto-segmentation where applicable (non-damaged retina). WT $NaIO_3$ 41.68 ± 3.86 μm *vs* TMEM97 KO $NaIO_3$: 20.49 ± 2.12 μm, $n = 4$, Student's *t*-test: $p = 0.0002$. RPE: retinal pigment epithelium. BM: Bruch's membrane. OS/IS: Photoreceptor outer and inner segments. ELM: external limiting membrane. ONL/INL: Outer and inner nuclear layer. GCL: Ganglion cell layer.

B. Exacerbated photoreceptor loss in KO *vs* WT retinas (histology). Eyeballs were collected at post-injection day 3 and fixed retinal sections were H&E stained. Red arrow marks the RPE layer. Yellow arrow points to intraretinal RPE migration. Scale bar: 50 μm. Quantification: Mean ± SEM, $n = 6$ mice; one-way ANOVA followed by Bonferroni test:

**$P < 0.01$. n.s., no significance. Note: A and B are separate experiments performed 6 months apart.

C. Increased ROS in KO *vs* WT retinas. TMEM97 KO and WT littermate mice received PBS or 30 mg/kg $NaIO_3$ through tail-vein injection, and non-fixed retinal cryosections from eyeballs collected at post-injection day 3 were used for ROS staining with H_2DCFDA. Shown for each condition are representative images from two animals. Scale bar: 50 μm.

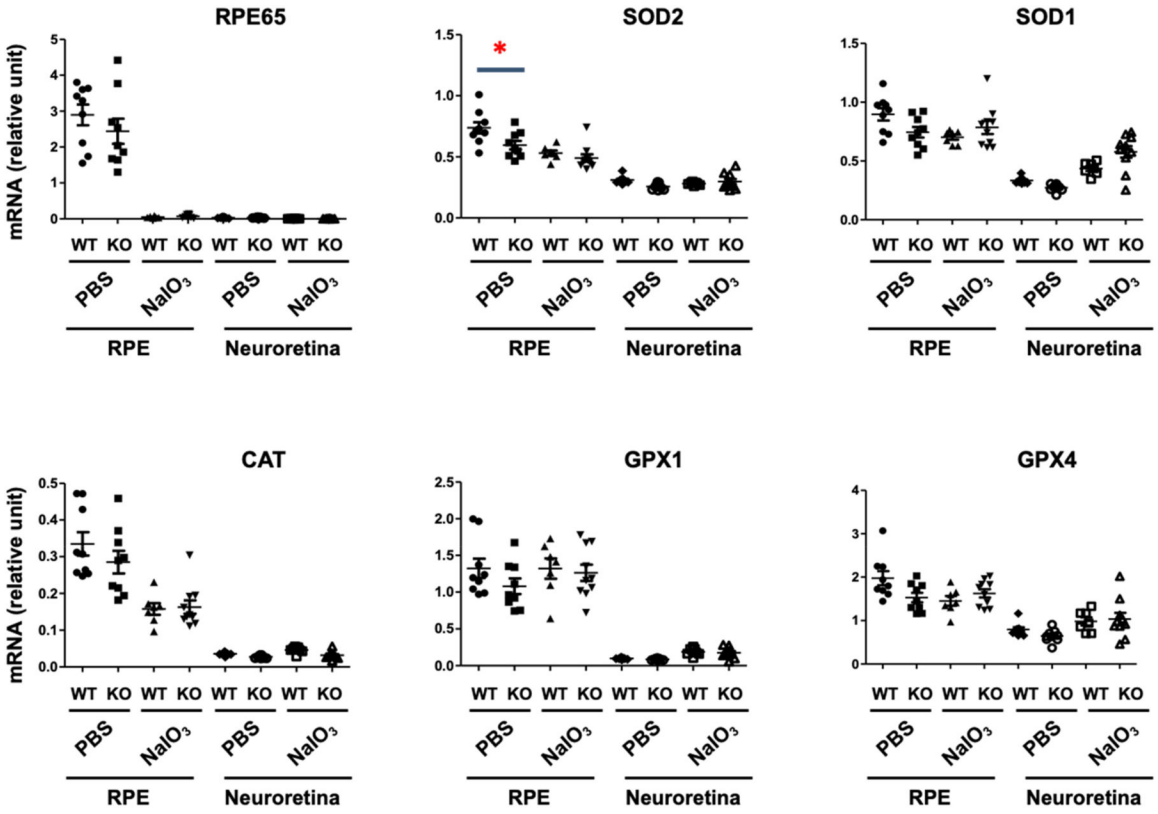

Fig. 3. Effect of TMEM97 KO on the expression of anti-oxidant enzymes in the RPE.

TMEM97 KO and WT littermate mice received PBS or 30 mg/kg $NaIO_3$ *via* tail-vein injection. The animals were euthanized at day 3 post-injection. The enucleated eye was dissected and the retina was carefully peeled off to avoid contamination with RPE. After gentle trituration with PBS in the eyecup, the RPE was collected. The retina and RPE tissue homogenates were used for total RNA extraction. qRT-PCR analysis: Data was normalized to *Gapdh* using the delta-delta Ct method. Mean ± SEM, $n = 7–8$ mice as indicated by the data points in the scatter plots. Statistics: One-way ANOVA followed by Bonferroni test: $*P < 0.05$. Non-significant comparison is not labeled. Note: This is an *in vivo* $NaIO_3$ treatment experiment separate from those in other figures.

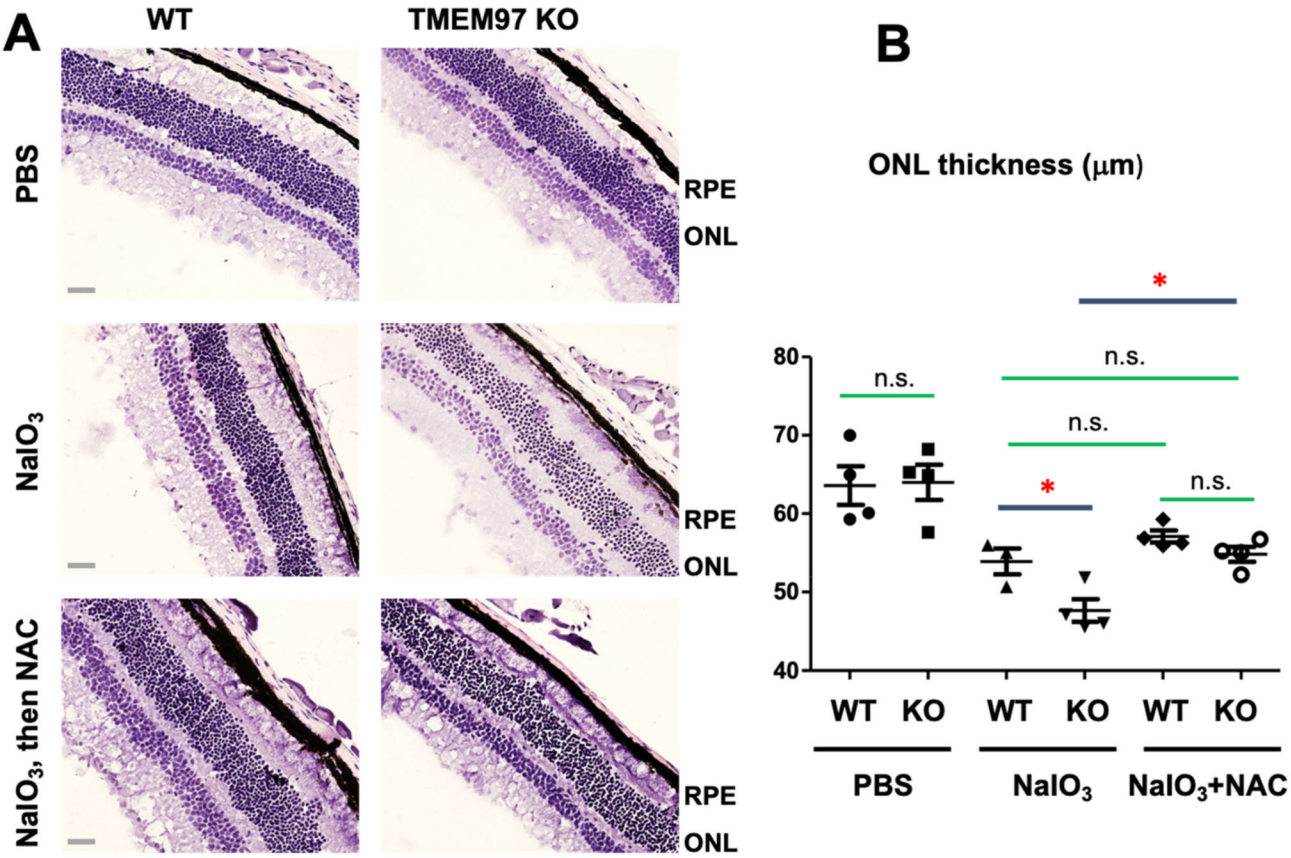

Fig. 4. Inhibition of TMEM97 KO-induced retinal degeneration by the anti-oxidant NAC.

A. Representative stained retinal cross-sections. TMEM97 KO and WT littermate mice received PBS or 30 mg/kg $NaIO_3$ *via* tail-vein injection. NAC was injected i.p. (200 mg/kg) every day for 3 days following $NaIO_3$ injection. Mouse eyes were collected at post-injection day 3 and fixed retinal sections were H&E stained. ONL: Outer nuclear layer. Scale bar: 50 μm.

B. Data quantification. Mean ± SEM; $n = 4$ mice as shown by the data points in the scatter plot; one-way ANOVA followed by Bonferroni test: $*P < 0.05$; n.s., no significance. Note: This and that in Fig. 2 are separate experiments performed in two different years.

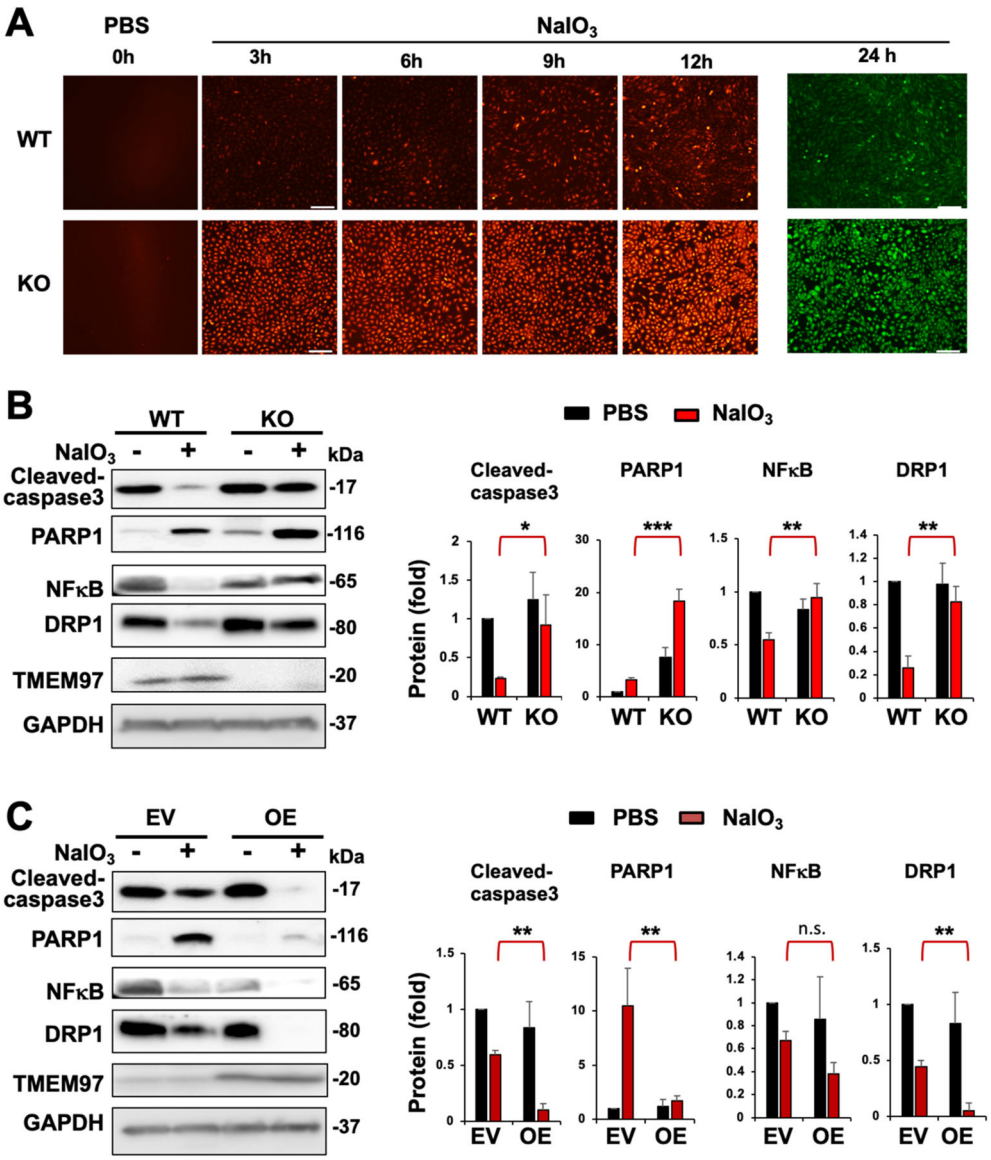

Fig. 5. Increased cellular ROS and degenerative phenotype markers in oxidatively challenged TMEM97 KO (*vs* WT) ARPE19 cells.

ARPE19 cells were cultured in DMEM/F12 (10% FBS) until >80% confluency. Cells were treated with PBS (control) or 5 mM $NaIO_3$ for indicated hours. At the end of treatment, the culture was changed to normal medium ($NaIO_3$-free), the fluorescent dye H_2DCFDA was then added to visualize intracellular ROS; otherwise cells were harvested for various assays. A. ROS upsurge in TMEM97 KO (*vs* WT) cells. The time course of increasing ROS in ARPE19 cells during $NaIO_3$ treatment was illuminated by staining with H_2DCFDA. Since the green fluorescence tended to be too strong, differential intensity (KO *vs* WT) was detected at Ex/m of 520/605 nm (red) for earlier time points and at 485/528 nm (green) at the 24 h time point. The PBS control is labeled as 0 h treatment. Scale bar: 50 μm
B. Western blot analysis for the impact of TMEM97 loss-of-function. $NaIO_3$ treatment: 5 mM for 24 h. NFκB: p65.

C. Western blot analysis for the impact of TMEM97 gain-of-function. EV: empty vector; OE: overexpression. $NaIO_3$ treatment: 5 mM for 24 h. NFκB: p65. Quantification for B and C: Mean ± SEM, $n \geq 3$ independent repeat experiments. Statistics: One-way ANOVA followed by Bonferroni test: *$P < 0.05$, **$P < 0.01$, ***$P < 0.001$, KO *vs* WT or OE *vs* EV (a pair of red bars). Non-significant comparisons are not labeled.

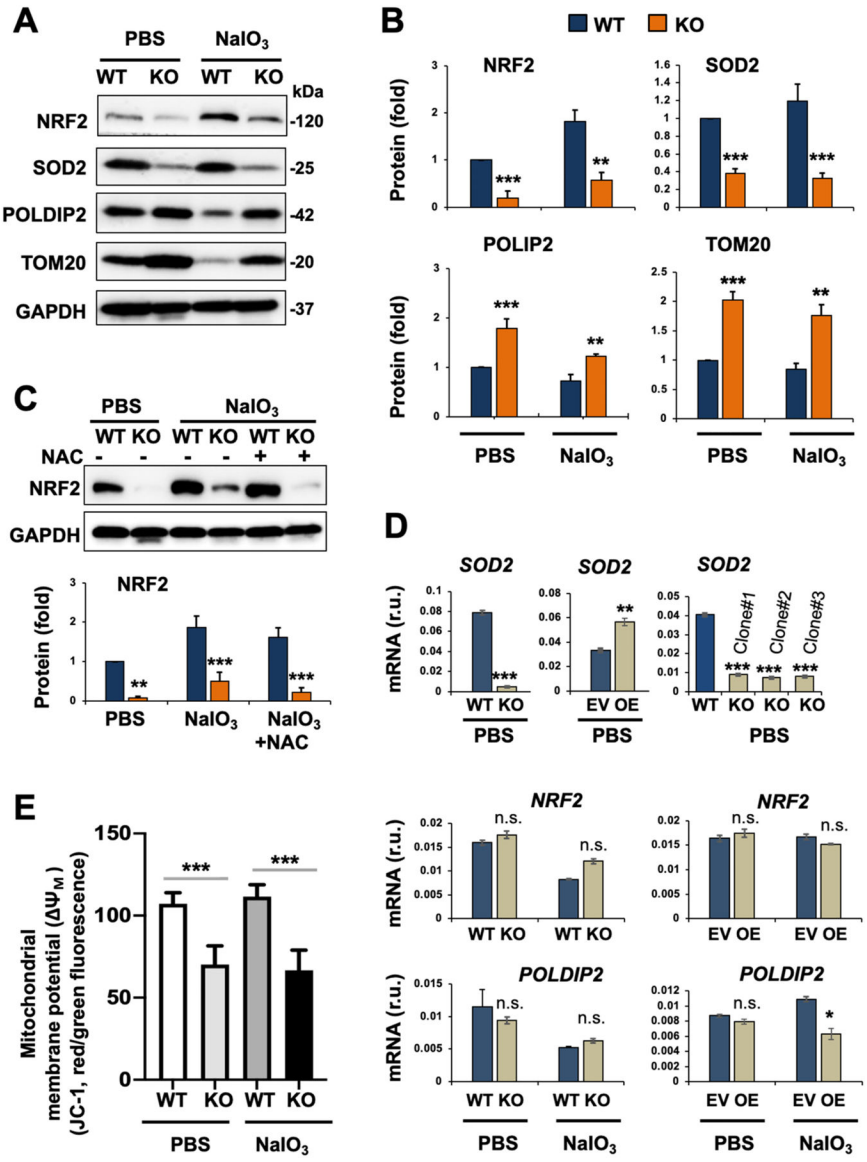

Fig. 6. Reduced NRF2 protein and altered mitochondria-residing (or associated) proteins in oxidatively challenged TMEM97 KO (*vs* WT) ARPE19 cells.

Prior to cell harvest for various assays, ARPE19 cells were treated with PBS or 5 mM $NaIO_3$ for 24 h, as described for Fig. 5. We chose to use the $NaIO_3$ condition of 5 mM/24 h in the remainder experiments of this study because it was sufficient to activate the apoptotic program yet without causing severe cell death so that various intracellular events could still be detected.

A. Representative Western blots.

B. Quantification for A: Mean ± SEM, $n = 6$ (for NRF2) and $n = 3$ independent repeat experiments (for other 3 proteins). Statistics: ANOVA followed by Bonferroni test: $^{*}P < 0.05$, $^{**}P < 0.01$, $^{***}P < 0.001$, KO *vs* WT. r.u., relative unit.

C. Lack of NAC effect on TMEM97 KO-induced NRF2 protein down-regulation. NAC was added together with $NaIO_3$. Quantification: Mean ± SEM, n = 3 independent repeat

experiments (different time than that in A/B). Statistics: ANOVA followed by Bonferroni test: ***$P < 0.001$ (KO *vs* WT).

D. qRT-PCR analysis. EV: empty vector; OE: overexpression. Quantification: Mean ± SD, n = triplicates. Statistics: ANOVA followed by Bonferroni test: *$P < 0.05$, **$P < 0.01$, ***P < 0.001, KO *vs* WT or OE *vs* EV. n.s., not significant. Shown in each plot is one of two similar experiments. Note: Among the three TMEM97 KO single clones, #1 was used for the rest of this study.

E. Mitochondrial membrane potential ($\Delta\Psi_M$). Assay was performed using the JC-1 kit (3 h $NaIO_3$ treatment). Quantification: Mean ± SD, n = triplicates. Statistics: ANOVA followed by Bonferroni test: ***$P < 0.001$ (KO *vs* WT).

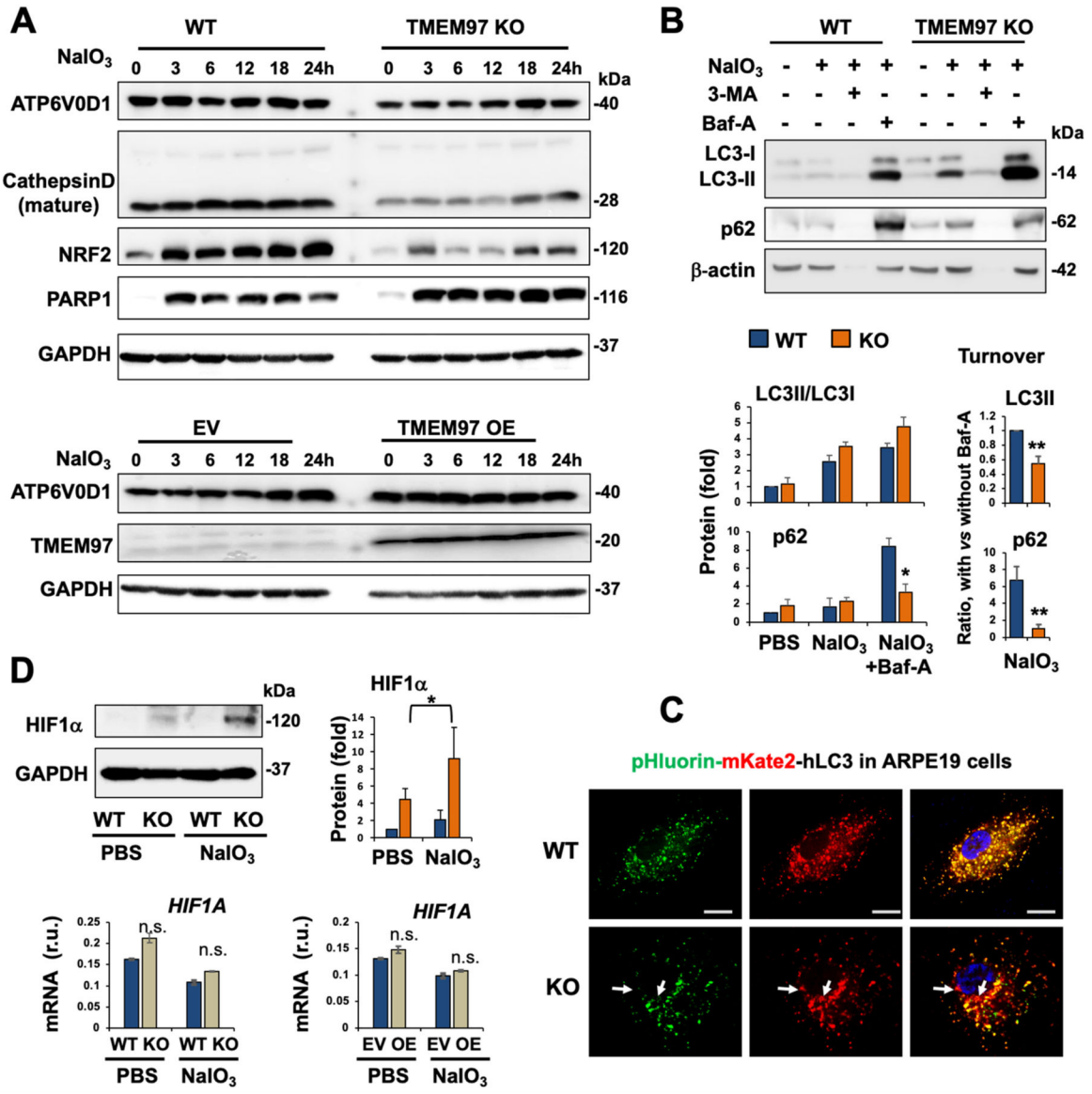

Fig. 7. Altered protein levels or turnover suggestive of compromised lysosomal function in oxidatively challenged TMEM97 KO (*vs* WT) ARPE19 cells.

Prior to cell harvest for various assays, ARPE19 cells were treated with PBS or 5 mM $NaIO_3$ for 24 h, as described for Fig. 5.

A. Time course of $NaIO_3$ treatment showing reduced ATP6V0D1 and cathepsin-D due to TMEM97 KO. NRF2 and PARP1 were also determined as positive controls for the impact of TMEM97 KO (as seen in Figs. 5 and 6).

B. Autophagosome cargo protein turnover. Cells were treated with PBS or $NaIO_3$, in the presence of vehicle (DMSO) or 10 μM 3-Methyladenine (3-MA, inhibitor of autophagosome biogenesis) or 50 nM bafilomycin-A (Baf-A, inhibitor of lysosomal function such as autophagosome-lysosome fusion). In the process of autophagic flux, LC3II and p62(SQSTM1) are transported to lysosomes *via* autophagosome-lysosome fusion and thereby degraded. Bafilomycin-A (Baf-A) blocks this lysosomal function. Thus, the difference or delta of the protein levels of p62 (or LC3II) with and without Baf-A measures

its turnover or autophagy flux. Note: 3-MA, blocker of autophagosome biogenesis, likely caused severe cell death (see beta-actin bands disappearing).

C. Analysis of autophagosome-lysosome fusion under oxidative stress of $NaIO_3$. Autophagosomes are indicated by pHluorin (GFP variant)-mKate2 (red) in tandem with LC3 (transfected into ARPE19 cells), which appeared as yellow puncta when not located in lysosomes; green (pHluorin) should be quenched inside lysosomes due to their lower pH, causing loss of green fluorescence. More red puncta (*e.g.* marked by white arrows) in KO *vs* WT cells suggest that autophagosome-lysosome fusion still occurred and that cargo has accumulated in lysosomes. Scale bar: 20 μm.

D. Increase of HIF1α protein (but not mRNA) in TMEM97 KO *vs* WT ARPE19 cells. Quantification of Western blots (for B and D): Mean ± SEM, n ≥ 3 independent repeat experiments. Quantification for qRT-PCR: Mean ± SD, n = triplicate. Statistics: ANOVA followed by Bonferroni test: $*P < 0.05$, $**P < 0.01$, KO *vs* WT.

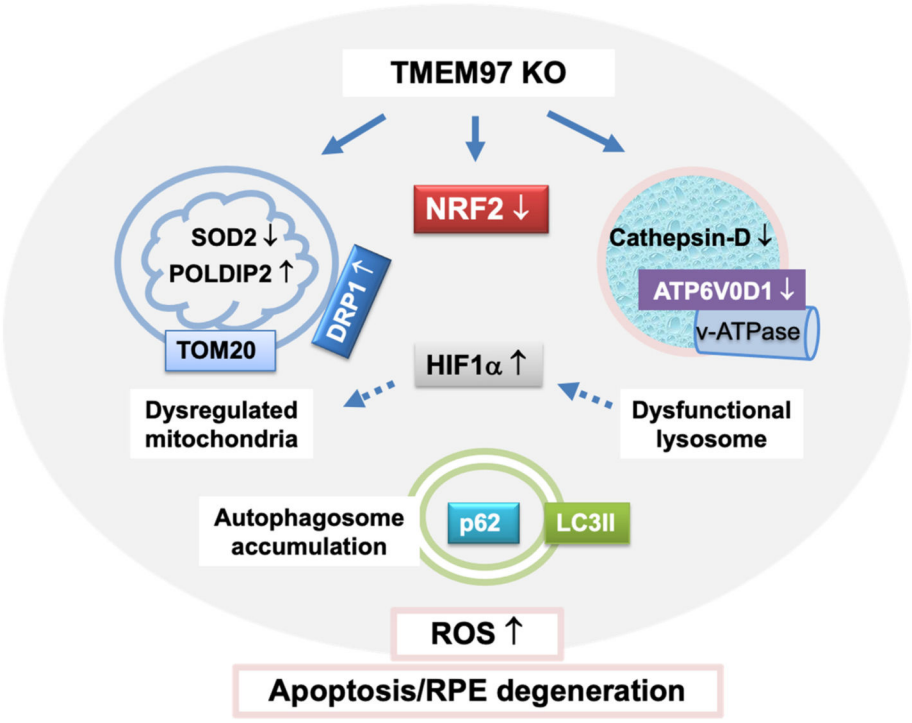

Fig. 8. Schematic working model.

The schematic hypothesis is based on the results from this study and also literature evidence. KO-induced changes (compared to WT) were observed in this study, including that in NRF2, HIF1α, SOD2, POLDIP2, TOM20, DRP1, ATP6V0D1, cathepsin-D protein levels, and p62/LC3II turnover rate; increase of HIF1α due to lysosomal dysfunction and its contribution to mitochondrial dysregulation (dashed arrows) are evidenced in the literature (cited in Discussion).